university of groningen

University Medical Center Groningen

University of Groningen

Substrate-Induced Conformational Changes in the S-Component ThiT from an Energy Coupling Factor Transporter

Majsnerowska, Maria; Hänelt, Inga; Wunnicke, Dorith; Schaefer, Lars V.; Steinhoff, Heinz-Juergen; Slotboom, Dirk Jan

Published in:
Structure

DOI:
10.1016/j.str.2013.03.007

IMPORTANT NOTE: You are advised to consult the publisher's version (publisher's PDF) if you wish to cite from it. Please check the document version below.

Document Version
Publisher's PDF, also known as Version of record

Publication date:
2013

Link to publication in University of Groningen/UMCG research database

Citation for published version (APA):
Majsnerowska, M., Hänelt, I., Wunnicke, D., Schaefer, L. V., Steinhoff, H-J., & Slotboom, D. J. (2013). Substrate-Induced Conformational Changes in the S-Component ThiT from an Energy Coupling Factor Transporter. *Structure*, *21*(5), 861-867. https://doi.org/10.1016/j.str.2013.03.007

Copyright
Other than for strictly personal use, it is not permitted to download or to forward/distribute the text or part of it without the consent of the author(s) and/or copyright holder(s), unless the work is under an open content license (like Creative Commons).

The publication may also be distributed here under the terms of Article 25fa of the Dutch Copyright Act, indicated by the "Taverne" license. More information can be found on the University of Groningen website: https://www.rug.nl/library/open-access/self-archiving-pure/taverne-amendment.

Take-down policy
If you believe that this document breaches copyright please contact us providing details, and we will remove access to the work immediately and investigate your claim.

Downloaded from the University of Groningen/UMCG research database (Pure): http://www.rug.nl/research/portal. For technical reasons the number of authors shown on this cover page is limited to 10 maximum.

Structure
Short Article

Substrate-Induced Conformational Changes in the S-Component ThiT from an Energy Coupling Factor Transporter

Maria Majsnerowska,[1,4] Inga Hänelt,[1,4] Dorith Wunnicke,[2,4] Lars V. Schäfer,[3] Heinz-Jürgen Steinhoff,[2] and Dirk Jan Slotboom[1,*]
[1]Department of Biochemistry, Groningen Biomolecular Sciences and Biotechnology Institute, Netherlands Proteomics Centre and Zernike Institute for Advanced Materials, University of Groningen, Nijenborgh 4, 9747 AG Groningen, The Netherlands
[2]Department of Physics, University of Osnabrueck, Barbarastrasse 7, 49076 Osnabrueck, Germany
[3]Institute of Physical and Theoretical Chemistry, Goethe-University Frankfurt, Max-von-Laue-Str. 7, D-60438 Frankfurt am Main, Germany
[4]These authors contributed equally to this work
*Correspondence: d.j.slotboom@rug.nl
http://dx.doi.org/10.1016/j.str.2013.03.007

SUMMARY

Energy coupling factor (ECF) transporters are a recently discovered class of ABC transporters that mediate vitamin uptake in prokaryotes. Characteristic for ECF-type ABC transporters are small integral membrane proteins (S-components) that bind the transported substrates with high affinity. S-components associate with a second membrane protein (EcfT) and two peripheral ATPases to form a complete ATP-dependent transporter. Here, we have used EPR spectroscopy, stopped-flow fluorescence spectroscopy, and molecular dynamics simulations to determine the structural rearrangements that take place in the S-component ThiT from *Lactococcus lactis* upon binding of thiamin. Thiamin-induced conformational changes were confined to the long and partially membrane-embedded loop between transmembrane helices 1 and 2 that acts as a lid to occlude the binding site. The results indicate that solitary ThiT functions as a bona fide high-affinity substrate binding protein, which lacks a translocation pathway within the protein.

INTRODUCTION

Energy coupling factor (ECF) proteins are ATP-binding cassette (ABC) transporters that mediate uptake of vitamins and trace elements in prokaryotes (Jeschke, 2012). They consist of two identical or homologous nucleotide-binding or ATPase subunits (EcfA), which are characteristic for the ABC transporter superfamily. The peripheral ATPase subunits form a complex, the ECF module, with the integral membrane protein EcfT. A second integral membrane protein (the S-component) is responsible for substrate binding and associates with the ECF module to form a functional ATP-dependent transporter (Figure 1C). ECF transporters do not make use of soluble substrate binding proteins/domains (SBP or SBD), which are usually part of bacterial ABC importers (Duurkens et al., 2007; Erkens and Slotboom, 2010; Erkens et al., 2011; Davidson et al., 2008).

Multiple S-components, specific for different substrates, can make use of the same ECF module (ter Beek et al., 2011; Rodionov et al., 2009). These different S-components usually share too little sequence similarity to establish homology. Nonetheless, the crystal structures of three S-components have revealed a similar fold: RibU (Protein Data Bank ID [PDB]: 3P5B) from *Staphylococcus aureus*, riboflavin-specific (Zhang et al., 2010) ThiT (for thiamin, PDB: 3RLB) (Erkens et al., 2011), and BioY (for biotin, PDB: 4DVE) (Berntsson et al., 2012), both from *Lactococcus lactis*. All have six transmembrane segments with cytoplasmic N and C termini. S-components bind their substrates with high affinity (dissociation constants below 1 nM) (Duurkens et al., 2007; Berntsson et al., 2012; Erkens and Slotboom, 2010). In the crystal structures of ThiT, BioY, and RibU, a substrate molecule (thiamin, biotin, and riboflavin, respectively) was found in an occluded site near the extracellular surface (Erkens et al., 2011; Berntsson et al., 2012; Zhang et al., 2010).

In vitro experiments have shown that solitary S-components, in the absence of the ECF module, can bind substrates but cannot translocate them across the membrane (Erkens et al., 2011; Zhang et al., 2010). In contrast, in vivo experiments on BioY from *Rhodobacter capsulatus* have suggested that the protein can also translocate biotin across the membrane (Hebbeln et al., 2007), although the data might alternatively be interpreted as ligand binding rather than transport (Berntsson et al., 2012). The structural basis for the potential translocation pathway was proposed based on the crystal structure of RibU (Zhang et al., 2010). Large structural rearrangements were postulated that could open a pathway that runs from the extracellular binding site (observed in all available crystal structures) to the cytoplasm in the presence of the ECF module. The rearrangements include substantial shifts in the relative positions of transmembrane helices. Here we have tested whether such large conformational changes take place in the absence of ECF module that would facilitate substrate translocation by solitary S-components. We have used the S-component ThiT rather than RibU, because of the crystal structure of ThiT is of higher resolution.

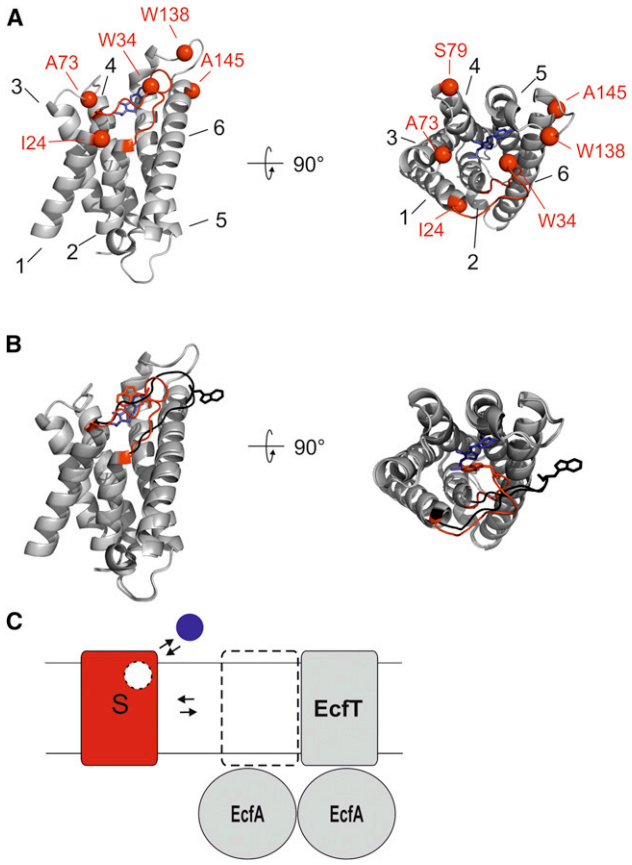

Figure 1. Structure of ThiT and Strategy for Spin-Labeling

(A) Crystal structure of ThiT with thiamin bound (PDB: 3RLB) with the C_α atoms of the residues that were used for spin labeling shown as red spheres. The transmembrane helices are numbered 1–6 (black numbers). Thiamin is shown as blue sticks.

(B) Overlay of ThiT with thiamin bound (crystal structure), and *apo*-ThiT using the distance constraints from the current study (detergent solubilized ThiT), illustrating the conformational changes of loop 1-2 upon thiamin binding. Loop 1-2 is colored red for liganded protein and black for thiamin-free protein. Tryptophan 34 and Thiamin are shown as black and blue sticks, respectively.

(C) Schematic organization of ECF transporters with substrate shown as blue circle.

See also Table S1.

We find that binding of thiamin to ThiT only requires opening of lid-like loop 1-2 that occludes the binding site whereas the transmembrane helices form a rigid scaffold. A translocation path for thiamin transport is absent in solitary ThiT.

RESULTS

To determine the nature and extent of the structural changes upon thiamin binding to ThiT we used electron paramagnetic resonance (EPR) spectroscopy. In the background of cysteine-less ThiT (C41A), we engineered pairs of cysteine residues, which were labeled with the methanethiosulfonate spin label MTSSL for EPR studies. We selected three positions for spin labeling in external loops (W34 in loop 1-2, A73 in loop 3-4, W138 in loop 5-6) and three in helices (I24, S79, and A145, in helix 1, 4, and 6, respectively), and combined them into seven pairs (Figure 1A). Position 34 in loop 1-2 was used in three pairs, in combination with positions 73, 79, and 145. Position 145 in helix 6 was combined with positions 24, 73, 79, and 138.

The distances between the spin labels in each of the purified ThiT variants were determined using continuous wave (cw) EPR spectroscopy (suitable for distances below 1.8 nm) and pulsed EPR methods (double electron electron resonance [DEER] spectroscopy, suitable for distances larger than 1.8 nm) (Joseph et al., 2011; Altenbach et al., 2008; Claxton et al., 2010; McHaourab et al., 2011; Hellmich et al., 2012; Jeschke, 2012) at low temperatures (160 K and 50 K, respectively). The experiments were done both in the presence and absence of thiamin, with the proteins in the detergent-solubilized state. In addition, selected spin-labeled mutants were analyzed in a membrane environment after reconstitution in liposomes.

For four ThiT variants (with spin label pairs at positions 73/145, 79/145, 138/145, and 24/145) thiamin binding did not affect the interspin distance (Figure 2A and Figure S1, available online; Table 1). The experimentally determined distances were in agreement with the simulated distances of the labeled protein based on the crystal structure of thiamin-bound ThiT (Erkens et al., 2011) (Figure S1A), although there were also differences (e.g., for the 24/145 pair). The latter indicates that the structure of the protein in solution is not identical to the crystal structure. Fluorescence titrations revealed that all spin-labeled variants were still capable of high-affinity thiamin binding (Table S1), which excludes the possibility that the lack of thiamin-induced distance changes was due to inactivation of ThiT, caused by the mutations or labeling.

Different results were obtained for variants with one of the spin labels located in extracellular loop 1-2. These variants all showed drastic changes in interspin distance upon substrate binding. The mean interspin distance between the labels at position 34 and 145 (located in loop 1-2 and helix 6, respectively) increased from 1.4 nm to 2.5 nm upon addition of thiamin, whereas the interspin distance for ThiT variants spin-labeled at positions 34/79 and 34/73 decreased upon thiamin addition (Figures 2A and S1; Table 1). These results show that loop 1-2 moves away from the thiamin binding site in the absence of thiamin. A structural model for the unliganded ThiT, in which we accounted for all the measured mean distances, is shown in Figure 1B.

We selected the ThiT variants with spin labels at positions 138/145, 34/79, and 34/73 to determine whether similar distance changes took place when the proteins were present in lipid bilayers after reconstitution in liposomes (Figures 2B and S1; Table 1). The distance between positions 138 and 145 was the same in the presence and absence of thiamin when the protein was reconstituted in liposomes, which is in agreement with the results of solubilized ThiT. The distances between the spin labels in the thiamin-bound variants 34/79 and 34/73 were smaller than in the thiamin-free protein, again consistent with the results obtained for the solubilized protein, and showing that loop 1-2 moved away from the thiamin binding site in the absence of substrate.

Although the direction of the distance change upon thiamin binding was the same in detergent solution and liposomes for the 34/79 and 34/73 variants, the absolute distances in the thiamin-free state differed. For 34/79 and 34/73 the mean

 ©2013 Elsevier Ltd All rights reserved

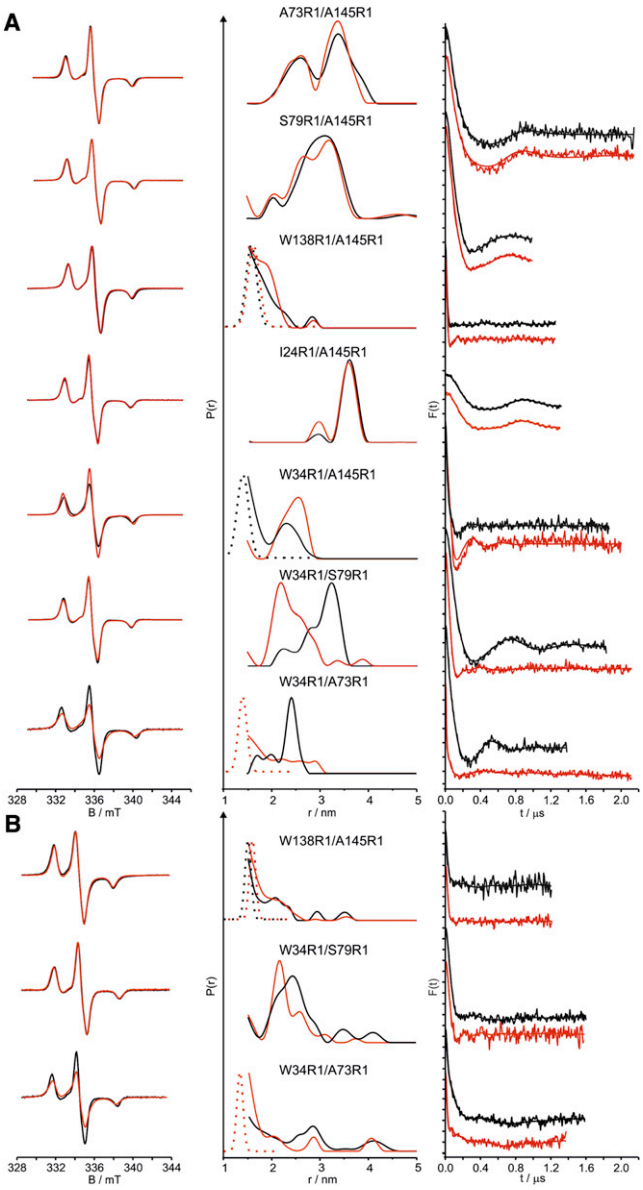

Figure 2. Interspin Distance Determination by cw and Pulse EPR Spectroscopy

(A and B) EPR measurements were done in the absence (black line) or presence (red line) of thiamin. Left: low temperature (160 K) spin normalized cw EPR spectra of doubly labeled ThiT variants. Center: distance distributions obtained from cw and pulse EPR measurements. The Gaussian distance distributions from the cw EPR measurements obtained by DipFit are indicated as dotted lines (Steinhoff et al., 1997) only for interspin distances in the 1–1.8 nm range. DEER-derived distributions in the P(r) panel are indicated as solid lines (Jeschke, 2012) for interspin distances above 1.8 nm. Right: background-corrected dipolar evolution data F(t). Tick marks are separated by 0.05. Solubilized ThiT variants (A) and ThiT variants reconstituted in liposomes (B). See also Figure S1.

distances between the spin labels measured in liposomes were 2.5 nm and 2.8 nm compared to 3.4 nm and 2.4 nm for the solubilized protein variants, respectively, showing that loop 1-2 adopts a slightly different conformation in the membrane environment than in the detergent micelle.

Table 1. Experimentally Determined Mean Interspin Distances between Spin-Labeled Residues in the Absence and in the Presence of Thiamin

Variant	Mean Distance in ThiT without Thiamin Bound (nm)	Mean Distance in ThiT with Thiamin Bound (nm)
A73R1/A145R1	2.6	2.6
	3.5	3.5
S79R1/A145R1	3.4	3.2
W138R1/A145R1	1.8 (1.5)	1.7 (1.6)
I24R1/A145R1	3.6	3.6
W34R1/A145R1	1.4	2.5
W34R1/A79R1	3.4 (2.5)	2.4 (2.1)
W34R1/A73R1	2.4 (2.8)	1.4 (1.4)

Values for the reconstituted protein are shown in parenthesis.

To further characterize the structure and dynamics of ThiT in the membrane we carried out all-atom molecular dynamics (MD) simulations of ThiT in a fully solvated POPC bilayer. The simulations provide an atomic-level picture of the changes of the protein structure in the presence and absence of thiamin, and help to interpret and validate the EPR data. The α helices of ThiT form a stable and rigid scaffold, both in the thiamin-bound and -free forms, as evidenced by the low root-mean-square deviation (rmsd) of the C_α-atoms compared to the crystal structure and low rms fluctuations (Figures 3, S2A, and S2B). The most pronounced differences between the simulations of thiamin-bound and -unbound ThiT were observed for the conformation of loop 1-2 (Figure 3). In the thiamin-bound structure, this loop seals off the binding pocket, with W34 being oriented inward (i.e., toward the center of the protein) and in direct contact with thiamin (Figure 3A, gray structure). In the absence of thiamin, loop 1-2 moves toward helix 6 and the W34 side chain changes orientation, now forming contacts with A149 and V150 in helix 6 (Figure 3A). As a consequence, W34, which in the thiamin-bound conformation is buried in the structure and thus largely shielded from the lipid environment, establishes more contacts with POPC lipids in the surrounding bilayer (Figure S2C). Similar structural rearrangements were observed in two additional, statistically independent MD simulations of *apo*-ThiT (of length 295 ns and 235 ns, respectively), whereas the protein conformation stayed close to the X-ray crystal structure during the two 300-ns MD simulations of the thiamin-bound form (Figures 3C and S2). The movement of loop 1-2 is depicted in Figures 3B and 3C, displaying the distance time-traces and distributions between residue pairs 34/79, 34/145, and 34/73, the same residue pairs that were used for spin labeling in the EPR studies. The distances between the other residue pairs (24/145, 73/145, 79/145, and 138/145) stayed very close to the respective distances in the crystal structure and did not depend on thiamin (Figures S2D and S2E), in agreement with the EPR results.

In the *apo*-protein, loops 3-4, 4-5, and 5-6 are equally flexible as loop 1-2 in terms of fluctuations (Figures 3A and S2B). Thus, the observation that the distances between A145 (helix 6) and either W138, located in loop 5-6, or A73, located in loop 3-4, are about the same in the thiamin-bound and -free states does not imply that the loops are rigid, but rather that large-amplitude

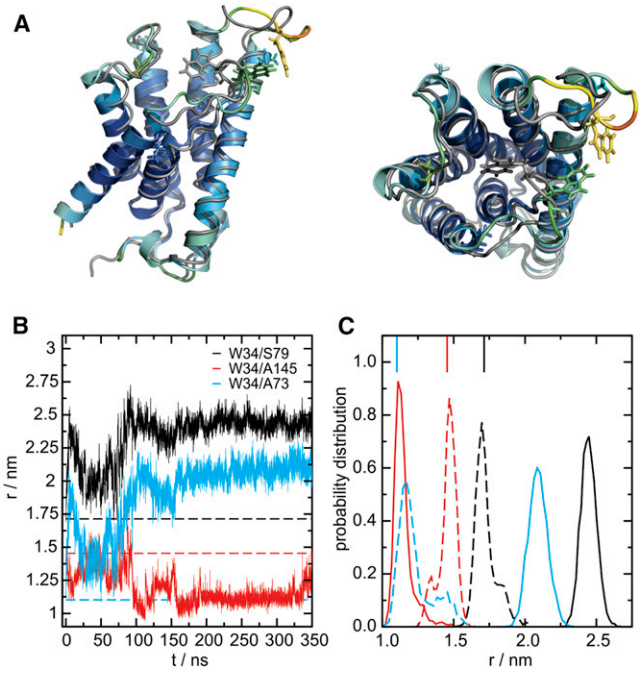

Figure 3. Molecular Dynamics Simulations

(A) Snapshot after 350 ns from MD simulation of *apo*-ThiT (no thiamin bound). The residues are colored according to their C_α-root-mean-square fluctuation (rmsf), from small (blue) to large rmsf (red). Residues labeled for EPR spectroscopy (I24, W34, A73, S79, W138, A145) are shown as sticks. POPC, water, and ions are not shown for clarity. The crystal structure of ThiT (PDB: 3RLB) is shown in gray.

(B) Time-traces of the distances between the centers of mass of residue pairs W34/S79 (black), W34/A145 (red), and W34/A73 (cyan) during a representative simulation of *apo*-ThiT.

(C) Distance distributions obtained from the last 100 ns of MD simulations in the absence (solid lines) and presence (dashed) of thiamin. The respective distances in the X-ray crystal structure are indicated by dashed lines in (B) and solid lines in (C), top.

See also Figure S2.

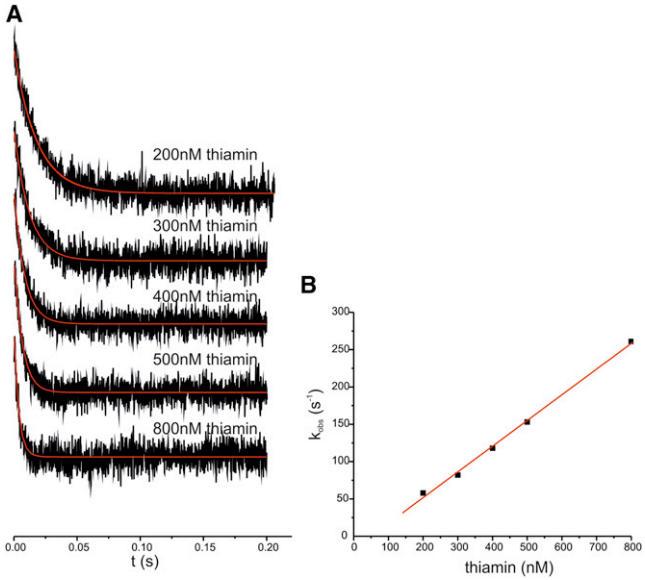

Figure 4. Rates of Thiamin Binding to WT ThiT

(A) Stopped flow tryptophan fluorescence measurements recorded after mixing of *apo*-ThiT with thiamin of indicated concentrations. Single-exponential fits are shown as red lines.

(B) Concentration dependence of the apparent rates (k_{obs}) of thiamin binding. The linear fit is shown as solid red line.

fluctuations yield structural ensembles with about the same mean distance. Because loops 3-4 and 5-6 lack residues involved in substrate binding, its motion does not contribute directly to the substrate binding kinetics.

The EPR distance measurements and MD simulations demonstrate that the conformational changes upon thiamin binding are restricted to loop 1-2 and do not lead to large structural rearrangements in the rest of the protein. To substantiate the localized nature of the structural changes, we determined the kinetic parameters of thiamin binding by stopped-flow fluorescence measurements. For these measurements, we made use of the quenching of tryptophan fluorescence that takes place when thiamin binds to ThiT. Fluorescence quenching occurred at the millisecond time scale upon mixing of 20 nM ThiT and thiamin (200–800 nM) (Figure 4A). Single exponential fits of the traces revealed the observed rate constants (k_{obs}). The k_{obs} values varied linearly with thiamin concentration (Figure 4B), allowing us to determine a k_{on} value of $3.4 \times 10^8\ M^{-1}s^{-1}$. The fast rate (near the diffusion limit) points to a small conformational rearrangement. The k_{on} is an order of magnitude faster than the k_{on} for sugar binding to periplasmic sugar binding proteins (Miller et al., 1983) or sialic acid binding protein (Müller et al., 2006) and two orders of magnitude faster than the k_{on} for peptide binding to OppA (Lanfermeijer et al., 1999). The latter proteins are unrelated to S-components and undergo more substantial conformational changes upon substrate binding, according to Venus flytrap model. The k_{off}, value was so low that it could not be determined accurately from the linear regression, because the intercept with the abscissa was too close to zero. k_{off} instead was calculated from the equilibrium dissociation constant ($k_d = k_{off}/k_{on}$,) and was found to be $0.04\ s^{-1}$.

DISCUSSION

The EPR spectroscopic data presented here show that the long and partially membrane-embedded extracytoplasmic loop 1-2 in ThiT undergoes a conformational change upon substrate binding. It is a lid on the binding site that—when open—allows access from the extracellular side of the membrane to the binding site, and—when closed—occludes the substrate. The MD simulations strongly support the conclusions of the EPR experiments and enable their interpretation at the atomic level. They show that, indeed, the transmembrane helices form a rigid scaffold that does not undergo large conformational changes upon thiamin binding whereas the loops are flexible. Loop 1-2 is directly involved in substrate binding.

Although the residue-to-residue centers of mass distances obtained from the MD simulations cannot be compared quantitatively to the EPR-derived distances between the NO-groups of the spin label side chains, both methods show the same trend. Both in the EPR measurements and in the MD simulations the distances between residue pairs 34/79 and 34/73 were larger in

the *apo*-protein than in the thiamin-bound form, whereas the 34/145 distance was smaller. The simulations also predict the formation of more contacts between W34 and lipids in the *apo*-state than in the thiamin-bound state. Consistent with this observation, the EPR distance measurements showed that loop 1-2 adopts a slightly different conformation in the membrane environment than in the detergent micelle (Figure 2). These results highlight the importance to address the possible effect of the lipid environment on membrane protein structure and function.

All the results presented here strongly support the view that solitary ThiT functions as a binding protein, which captures its substrate with a rate close to the diffusion limit and extremely rarely allows its release. A low off-rate for biotin release from BioY had been indicated by binding assays in proteoliposomes (Berntsson et al., 2012) and is consistent with the k_{off} measured for ThiT here (0.04 s^{-1}). There are no indications that large structural rearrangements take place that would be required to open a translocation pathway within the S-component as was suggested for RibU. However, in complex with the ECF module, we expect that additional conformational changes take place in the S-components, which allow for substrate translocation. Whether a pathway is then formed within the S-component, at the interface between the S-component and the ECF module, or within the ECF module remains to be determined.

EXPERIMENTAL PROCEDURES

Plasmids Construction

Plasmids containing mutations in the gene encoding ThiT were generated from plasmid pREnHis-ThiT (Erkens and Slotboom, 2010) by PCR using the QuikChange method (Stratagene). The pREnHis-ThiT mutants were converted into expression vectors for *L. lactis* (pNZ plasmids) using the vector backbone exchange (VBEx) protocol (Geertsma and Poolman, 2007). All plasmids were verified by DNA sequencing (Seqlab, Germany).

Overexpression, Purification, and Spin Labeling of ThiT Mutants

L. lactis strain NZ9000 containing pNZnHis-ThiT variants were grown semi-anaerobically in 1 l bottles at 30°C using either chemically defined medium (Berntsson et al., 2009) without thiamin, to obtain substrate-free protein (Erkens and Slotboom, 2010), or M17 broth (Difco), to obtain liganded protein. Both growth media were supplemented with 1.5% (w/v) glucose and 5 μg/ml chloramphenicol. Expression was induced at an OD_{600} of 1.0 by the addition of 0.1% (v/v) of the culture supernatant from the Nisin A producing strain NZ9700 (Kuipers et al., 1998). The cells were allowed to continue growing for 2 hr and harvested at a final OD_{600} of 2.5–3.5. Cells were broken and membrane vesicles were prepared as described (Erkens and Slotboom, 2010). The previously described purification protocol (Erkens et al., 2011) was modified as follows: 50 mM potassium phosphate (KP_i) buffer pH 7.0 supplemented with 150 mM KCl was used throughout the purification. Membrane vesicles were solubilized in 1.0% (w/v) n-dodecyl-β-d-maltopyranoside (DDM, Anatrace), but in all subsequent steps 0.15% n-decyl-β-d-maltopyranoside (DM, Anatrace) was used. Two washing steps were performed when the protein was bound to the Ni-Sepharose column: the first with 20 column volumes (CV) of washing buffer containing 5 mM β-mercaptoethanol (to reduce all sulfhydryl groups) and the second with 20 CV degassed washing buffer (to remove reducing agent). The ThiT variants were spin-labeled during purification on the Ni-Sepharose. The protein was incubated overnight at 4°C with 1 mM spin label (1-oxyl-2,2,5,5-tetramethlpyrroline-3-methyl)- methanethiosulfonate (TRC, Toronto, Canada) dissolved in washing buffer. Free spin label was washed away with 20 CV of washing buffer.

The peak fractions after size exclusion chromatography were concentrated on a Vivaspin 30-kDa molecular weight cutoff concentrator (GE Healthcare) to 2–3 mg/ml. During concentration the size-exclusion chromatography (SEC) buffer (50 mM KPi pH 7.0, 150 mM KCl, 0.15% DM) was exchanged for SEC buffer with D_2O instead of H_2O. Concentrated ThiT variants were used for EPR measurements and supplemented with 20% D_2-glycerol and 100 μM thiamin if indicated.

Reconstitution into Liposomes

Purified and spin-labeled ThiT was reconstituted into liposomes prepared from a 3:1:1 molar ratio of 1,2-dioleoyl-*sn*-glycero-3-phosphoethanolamine (DOPE):1,2-dioleoyl-*sn*-glycero-3-phosphocholine (DOPC):1,2-dioleoyl-*sn*-glycero-3-phospho-(1′-*rac*-glycerol) (DOPG) (Avanti Polar Lipids) at a protein:lipid ratio of 1:20 (w/w) according to the previously described protocol (Groeneveld and Slotboom, 2010). Proteoliposomes were resuspended in 50 mM KP_i buffer pH 7.0 with D_2O plus 20% D_2-glycerol at a lipid concentration of 40 mg/ml.

Fluorescence Measurements

Steady-state Trp fluorescence measurements were performed in SEC buffer with 50 nM protein concentration (Erkens and Slotboom, 2010).

Stopped flow measurements were performed at 25°C on an Applied Photophysics SX20 spectrometer using excitation wavelength of 280 nm and a 310 nm cutoff filter for emission. Measurements were done in SEC buffer with 20 nM final protein concentration. Seven to nine traces were recorded (for each substrate concentration), averaged, and fitted to a single exponential decay function of the form $F_t = \Delta F + A \times \exp(-k_{obs} \times t)$, where F_t denotes the fluorescence at time t, ΔF is the fluorescence quenching after completion of the binding reaction, A is the signal amplitude, and k_{obs} is the observed rate constant. Fitting was performed in Origin 7.0 (OriginLab) to obtain a value for k_{obs}.

EPR Measurements

Low temperature (160 K) cw EPR spectra at X band were carried out using a homemade EPR spectrometer equipped with a Super High Sensitivity Probehead (Bruker) (microwave power: 0.2 mW, B-field modulation amplitude: 0.25 mT). Temperature stabilization was achieved by a continuous flow helium cryostat (ESR 900, Oxford Instruments) in combination with a temperature controller (ITC 503S, Oxford Instruments). A RMN 2 B-field meter (Drusch) allowed measurement of the magnetic field. Sample volumes of 30–40 μl were loaded into EPR quartz capillaries and frozen in liquid nitrogen before insertion into the resonator.

Pulse EPR measurements were performed at X-band frequencies using a Bruker Elexsys 580 spectrometer equipped with a 3-mm split ring resonator (ER 4118X-MS3, Bruker). A continuous flow cryostat (ESR900, Oxford Instruments) in combination with a temperature controller (ITC 503S, Oxford Instruments) was used for temperature stabilization. Sample volumes of 30–40 μl were loaded into EPR quartz capillaries and frozen in liquid nitrogen. The four-pulse DEER sequence $\pi/2(\nu_{obs}) - \tau_1 - \pi(\nu_{obs}) - \tau' - \pi(\nu_{pump}) - (\tau_1 + \tau_2 - t') - \pi(\nu_{obs}) - \tau_2 -$ echo was applied (Pannier et al., 2000). A two-step phase cycling $(+\langle x\rangle, -\langle x\rangle)$ was realized on $\pi/2(\nu_{obs})$, whereas for all pulses at the observer frequency the $\langle x\rangle$ channels were applied. The pump frequency ν_{pump} was positioned at the center of the resonator dip corresponding to the maximum of the echo-detected nitroxide EPR absorption spectrum, whereas the observer frequency ν_{obs} was set to the low field local maximum of the absorption spectrum resulting in a 65 MHz offset. The pump pulse possessed a length of 12 ns and the observer pulses lengths of 16 ns for $\pi/2$ and 32 ns for π pulses. The dipolar evolution time was given by $t = t' - \tau_1$. Time t' was varied, whereas τ_1 and τ_2 were kept constant and data with $t > 0$ were analyzed. Deuterium modulation was averaged by adding traces at eight different τ_1 start values, starting at $\tau_{1,0} = 200$ ns and incrementing by $\Delta\tau_1 = 56$ ns.

Fitting of Experimental cw EPR Data

Simulated dipolar broadened EPR spectra were fitted to experimental low temperature cw EPR spectra using the program DipFit (Steinhoff et al., 1997). DipFit determines best-fit parameters for the interspin distance and distance distribution considering a Gaussian distribution of distances. During the fitting procedure the g tensor values, the A_{xx} and A_{yy} values of the hyperfine tensor and the Lorentzian and Gaussian line width parameters are fixed to $g_{xx} = 2.0082$, $g_{yy} = 2.0063$, $g_{zz} = 2.0024$, $A_{xx} = 0.45$ mT, and $A_{yy} = 0.46$ mT. EPR spectra are convoluted with a field-independent line shape function composed of a superposition of 52% Lorentzian and 48% Gaussian of 0.25 and 0.31 mT widths, respectively.

Analysis of Pulse EPR Data

For analyzing the pulse EPR data the experimental echo decay was background-corrected using a homogeneous 3.0–3.9-dimensional spin distribution. Interspin distance distributions were derived by fitting the background-corrected dipolar evolution function using Tikhonov regularization as implemented in DEERAnalysis2008 (Polyhach et al., 2011).

Simulations of Distance Distributions

Interspin distance distributions were simulated using an approach based on a rotamer library as implemented in the program MMM (Polyhach et al., 2011). The rotamer library contains 210 precalculated rotamers representing an ensemble of possible spin label side chain (R1) conformations. The orientation of the spin label side chain introduced at a specific residue with regard to the protein structure permits calculation of the energy for the R1-protein interaction in consideration of the Lennard Jones potential (Mackerell et al., 2004). An adjacent Boltzmann weighting and normalization by the partition function results in the probability for each rotamer. Multiplication of the probability for each rotamer with the probability of R1 to exhibit this conformation leads to the rotamer probability distribution for the specific residue. Interspin distance distributions are calculated as the histogram of all pairwise interspin distances weighted by the product of their respective probabilities.

Molecular Modeling

The starting structure for the unliganded ThiT model was the crystal structure of thiamin-bound ThiT (Erkens et al., 2011). The initial molecular structure was fixed except for loop 1-2 that was rearranged on the basis of the experimentally determined interspin distances using the program Yasara (Krieger et al., 2002). Finally, the unliganded ThiT model was energy minimized using the minimization experiment provided by Yasara Dynamics.

MD Simulations

MD simulations were carried out with the GROMACS program package, v4.5 (Hess et al., 2008). A ThiT monomer, taken from the crystal structure (PDB: 3RLB) (Erkens et al., 2011), was simulated a fully solvated palmitoyloleoylphosphatidylcholine (POPC) lipid bilayer. For the simulations of *apo*-ThiT, thiamin was removed from the PDB structure. The periodic simulation box contained 248 POPC lipids (124 in each leaflet), ~17,660 TIP3P water (Jorgensen et al., 1983) molecules, and 55 Cl^- and 46 Na^+ ions (47 Na^+ in case of the *apo*-protein lacking the thiamin cation) to neutralize the simulation box. The box xyz-dimensions were ~9.2 × 8.8 × 10.6 nm. The AMBER99SB force field (Hornak et al., 2006) was used for the protein, together with the Berger lipid parameters (Berger et al., 1997), including the dihedral parameters by Bachar et al. (2004) for the torsion around the bond adjacent to the *cis* double bond in the POPC hydrocarbon tail; the lipid parameters were obtained from Cordomi et al. (2012). For the Na^+ and Cl^- ions, the parameters of Joung and Cheatham (2008) were applied. The thiamin parameters were obtained from the general AMBER force field (GAFF) (Wang et al., 2004). Long-range electrostatic interactions were treated with the particle-mesh-Ewald (PME) method (Darden et al., 1993) with a grid-spacing of 0.12 nm. Short-range van der Waals interactions were described with a Lennard-Jones 6-12 potential that was cut-off at 1.0 nm. The nonbonded neighbor list was updated every 16 fs within this cut-off. Analytic corrections to the pressure and potential energy were applied to compensate for the truncation of the Lennard-Jones interactions (Allen and Tildesley, 1989). The SETTLE algorithm (Miyamoto and Kollman, 1992) was used to constrain the bonds and angles of the water molecules, and LINCS (Hess, 2008; Hess et al., 1997) was used to constrain all other bond lengths. The integration time step was 2 fs for the simulations with thiamin. For *apo*-ThiT, virtual interaction sites were used for the hydrogen atoms (Feenstra et al., 1999), allowing for an integration time step of 4 fs. The temperature was kept constant at 300 K by coupling to a velocity rescaling thermostat (Bussi et al., 2007) with coupling time constant 0.1 ps. For constant pressure, semi-isotropic coupling was applied by separately coupling the lateral (xy) and normal (z) directions to a pressure bath at 1 bar using a Berendsen barostat with a time constant of 0.5 ps and compressibility 4.5 × 10^{-5} bar^{-1}.

Thiamin GAFF parameters were obtained using the ANTECHAMBER program as part of the AMBER tools. The electrostatic potential (ESP) of thiamin in vacuo was calculated from a Hartree-Fock/6-31G(d) wavefunction with the Merz-Singh-Kollman scheme (Chandra Singh and Kollman, 1984) after geometry optimization at the B3LYP/6-31G(d) density functional level of theory using the GAUSSIAN09 software package. The final partial charges were determined with the RESP method (Bayly et al., 1993), as implemented in ANTECHAMBER. The AMBER topology was converted to GROMACS format with the amb2gmx.pl script (Mobley et al., 2006) downloaded from http://ffamber.cnsm.csulb.edu.

To determine the orientation and insertion of the protein in the lipid bilayer, the orientations of proteins in membranes (OPM) web server (Lomize et al., 2012) was used. The oriented protein was inserted into a pre-equilibrated POPC bilayer using the inflation/deflation protocol of Kandt et al. (2007). All crystallographic water molecules were kept during the preparation of the structure for MD simulations. The protein-bilayer system was solvated with water such that no water molecules were introduced in the hydrocarbon region of the bilayer, and Na^+ and Cl^- ions were added in the bulk water. The system was then energy minimized (1,000 steps steepest descent). Subsequently, the system temperature was linearly raised from 60 to 300 K during 100 ps, followed by 6 ns equilibration at 300 K. During these simulations, harmonic position restraints with force constants 1,000 kJ mol^{-1} nm^{-2} were applied to all protein heavy atoms. Finally, the position restraints were released during nine subsequent 100-ps simulations by decreasing the force constants in steps of 100 kJ mol^{-1} nm^{-2}. Thus, the overall equilibration time prior to the production simulations was 7 ns. This relatively long equilibration time was chosen to allow the relaxation of the lipid and water molecules, and, for *apo*-ThiT, the wetting of the binding pocket. Both is the case, as evident from the time evolution of the simulation box vectors and potential energy of the system, and close visual inspection. For *apo*-ThiT, three statistically independent production MD simulations (of length 350 ns, 295 ns, and 235 ns, respectively) were initiated by choosing different random seeds for the initial Maxwell velocity distribution at 300 K. Similarly, two independent 300-ns simulations were carried out for the thiamin-bound form. Thus, altogether, the overall simulation time is ~1.5 μs.

SUPPLEMENTAL INFORMATION

Supplemental Information includes two figures and one table and can be found with this article online at http://dx.doi.org/10.1016/j.str.2013.03.007.

ACKNOWLEDGMENTS

This work was supported by grants from The Netherlands Organisation for Scientific research (NWO: Vici and ALW Open Program grants to D.J.S.), the EU (ERC starting grant to D.J.S. and EDICT program), and the Deutsche Forschungsgemeinschaft (postdoctoral fellowship to I.H., grant STE 640/10 to H.J.S., and Emmy Noether grant to L.V.S.). We thank Arnau Cordomi for sharing the POPC force field parameters.

Received: October 24, 2012
Revised: February 20, 2013
Accepted: March 8, 2013
Published: April 18, 2013

REFERENCES

Allen, M.P., and Tildesley, D.J. (1989). Computer Simulation of Liquids (USA: Oxford University Press).

Altenbach, C., Kusnetzow, A.K., Ernst, O.P., Hofmann, K.P., and Hubbell, W.L. (2008). High-resolution distance mapping in rhodopsin reveals the pattern of helix movement due to activation. Proc. Natl. Acad. Sci. USA *105*, 7439–7444.

Bachar, M., Brunelle, P., Tieleman, D.P., and Rauk, A. (2004). Molecular dynamics simulation of a polyunsaturated lipid bilayer susceptible to lipid peroxidation. J. Phys. Chem. B *108*, 7170–7179.

Bayly, C.I., Cieplak, P., Cornell, W.D., and Kollman, P.A. (1993). A well-behaved electrostatic potential based method using charge restraints for deriving atomic charges: the RESP model. J. Phys. Chem. *97*, 10269–10280.

Berger, O., Edholm, O., and Jähnig, F. (1997). Molecular dynamics simulations of a fluid bilayer of dipalmitoylphosphatidylcholine at full hydration, constant pressure, and constant temperature. Biophys. J. *72*, 2002–2013.

 ©2013 Elsevier Ltd All rights reserved

Berntsson, R.P.-A., Alia Oktaviani, N., Fusetti, F., Thunnissen, A.-M.W.H., Poolman, B., and Slotboom, D.J. (2009). Selenomethionine incorporation in proteins expressed in Lactococcus lactis. Protein Sci. *18*, 1121–1127.

Berntsson, R.P.-A., ter Beek, J., Majsnerowska, M., Duurkens, R.H., Puri, P., Poolman, B., and Slotboom, D.J. (2012). Structural divergence of paralogous S components from ECF-type ABC transporters. Proc. Natl. Acad. Sci. USA *109*, 13990–13995.

Bussi, G., Donadio, D., and Parrinello, M. (2007). Canonical sampling through velocity rescaling. J. Chem. Physiol. *126*, 014101.

Chandra Singh, U., and Kollman, P.A. (1984). An approach to computing electrostatic charges for molecules. J. Comput. Chem. *5*, 129–145.

Claxton, D.P., Quick, M., Shi, L., de Carvalho, F.D., Weinstein, H., Javitch, J.A., and McHaourab, H.S. (2010). Ion/substrate-dependent conformational dynamics of a bacterial homolog of neurotransmitter:sodium symporters. Nat. Struct. Mol. Biol. *17*, 822–829.

Cordomi, A., Caltabiano, G., and Pardo, L. (2012). Membrane protein simulations using AMBER force field and Berger lipid parameters. J. Chem. Theory Comput. *8*, 948–958.

Darden, T., York, D., and Pedersen, L. (1993). Particle mesh Ewald: an N·log(N) method for Ewald sums in large systems. J. Chem. Phys. *98*, 10089.

Davidson, A.L., Dassa, E., Orelle, C., and Chen, J. (2008). Structure, function, and evolution of bacterial ATP-binding cassette systems. Microbiol. Mol. Biol. Rev. *72*, 317–364.

Duurkens, R.H., Tol, M.B., Geertsma, E.R., Permentier, H.P., and Slotboom, D.J. (2007). Flavin binding to the high affinity riboflavin transporter RibU. J. Biol. Chem. *282*, 10380–10386.

Erkens, G.B., and Slotboom, D.J. (2010). Biochemical characterization of ThiT from Lactococcus lactis: a thiamin transporter with picomolar substrate binding affinity. Biochemistry *49*, 3203–3212.

Erkens, G.B., Berntsson, R.P.A., Fulyani, F., Majsnerowska, M., Vujičić-Žagar, A., ter Beek, J., Poolman, B., and Slotboom, D.J. (2011). The structural basis of modularity in ECF-type ABC transporters. Nat. Struct. Mol. Biol. *18*, 755–760.

Feenstra, K.A., Hess, B., and Berendsen, H.J.C. (1999). Improving efficiency of large time-scale molecular dynamics simulations of hydrogen-rich systems. J. Comput. Chem. *20*, 786–798.

Geertsma, E.R., and Poolman, B. (2007). High-throughput cloning and expression in recalcitrant bacteria. Nat. Methods *4*, 705–707.

Groeneveld, M., and Slotboom, D.J. (2010). Na(+):aspartate coupling stoichiometry in the glutamate transporter homologue Glt(Ph). Biochemistry *49*, 3511–3513.

Hebbeln, P., Rodionov, D.A., Alfandega, A., and Eitinger, T. (2007). Biotin uptake in prokaryotes by solute transporters with an optional ATP-binding cassette-containing module. Proc. Natl. Acad. Sci. USA *104*, 2909–2914.

Hellmich, U.A., Lyubenova, S., Kaltenborn, E., Doshi, R., van Veen, H.W., Prisner, T.F., and Glaubitz, C. (2012). Probing the ATP hydrolysis cycle of the ABC multidrug transporter LmrA by pulsed EPR spectroscopy. J. Am. Chem. Soc. *134*, 5857–5862.

Hess, B. (2008). P-LINCS: a parallel linear constraint solver for molecular simulation. J. Chem. Theory Comput. *4*, 116–122.

Hess, B., Bekker, H., Berendsen, H.J.D., and Fraaije, J.G.E.M. (1997). LINCS: a linear constraint solver for molecular simulations. J. Comput. Chem. *18*, 1463–1472.

Hess, B., Kutzner, C., van der Spoel, D., and Lindahl, E. (2008). GROMACS 4: algorithms for highly efficient, load-balanced, and scalable molecular simulation. J. Chem. Theory Comput. *4*, 435–447.

Hornak, V., Abel, R., Okur, A., Strockbine, B., Roitberg, A., and Simmerling, C. (2006). Comparison of multiple Amber force fields and development of improved protein backbone parameters. Proteins *65*, 712–725.

Jeschke, G. (2012). DEER distance measurements on proteins. Annu. Rev. Phys. Chem. *63*, 419–446.

Jorgensen, W.L., Chandrasekhar, J., Madura, J.D., Impey, R.W., and Klein, M.L. (1983). Comparison of simple potential functions for simulating liquid water. J. Chem. Phys. *79*, 926–935.

Joseph, B., Jeschke, G., Goetz, B.A., Locher, K.P., and Bordignon, E. (2011). Transmembrane gate movements in the type II ATP-binding cassette (ABC) importer BtuCD-F during nucleotide cycle. J. Biol. Chem. *286*, 41008–41017.

Joung, I.S., and Cheatham, T.E., 3rd. (2008). Determination of alkali and halide monovalent ion parameters for use in explicitly solvated biomolecular simulations. J. Phys. Chem. B *112*, 9020–9041.

Kandt, C., Ash, W.L., and Tieleman, D.P. (2007). Setting up and running molecular dynamics simulations of membrane proteins. Methods *41*, 475–488.

Krieger, E., Koraimann, G., and Vriend, G. (2002). Increasing the precision of comparative models with YASARA NOVA—a self-parameterizing force field. Proteins *47*, 393–402.

Kuipers, O.P., de Ruyter, P.G.G.A., Kleerebezem, M., and Voss, W.M. (1998). Quorum sensing-controlled gene expression in lactic acid bacteria. J. Biotech. *64*, 15–21.

Lanfermeijer, F.C., Picon, A., Konings, W.N., and Poolman, B. (1999). Kinetics and consequences of binding of nona- and dodecapeptides to the oligopeptide binding protein (OppA) of Lactococcus lactis. Biochemistry *38*, 14440–14450.

Lomize, M.A., Pogozheva, I.D., Joo, H., Mosberg, H.I., and Lomize, A.L. (2012). OPM database and PPM web server: resources for positioning of proteins in membranes. Nucleic Acids Res. *40*(Database issue), D370–D376.

Mackerell, A.D., Jr., Feig, M., and Brooks, C.L., 3rd. (2004). Extending the treatment of backbone energetics in protein force fields: limitations of gas-phase quantum mechanics in reproducing protein conformational distributions in molecular dynamics simulations. J. Comput. Chem. *25*, 1400–1415.

McHaourab, H.S., Steed, P.R., and Kazmier, K. (2011). Toward the fourth dimension of membrane protein structure: insight into dynamics from spin-labeling EPR spectroscopy. Structure *19*, 1549–1561.

Miller, D.M., 3rd, Olson, J.S., Pflugrath, J.W., and Quiocho, F.A. (1983). Rates of ligand binding to periplasmic proteins involved in bacterial transport and chemotaxis. J. Biol. Chem. *258*, 13665–13672.

Miyamoto, S., and Kollman, P.A. (1992). SETTLE—an analytical version of the SHAKE and RATTLE algorithm for rigid water models. J. Comput. Chem. *13*, 952–962.

Mobley, D.L., Chodera, J.D., and Dill, K.A. (2006). On the use of orientational restraints and symmetry corrections in alchemical free energy calculations. J. Chem. Phys *125*, 084902.

Müller, A., Severi, E., Mulligan, C., Watts, A.G., Kelly, D.J., Wilson, K.S., Wilkinson, A.J., and Thomas, G.H. (2006). Conservation of structure and mechanism in primary and secondary transporters exemplified by SiaP, a sialic acid binding virulence factor from Haemophilus influenzae. J. Biol. Chem. *281*, 22212–22222.

Pannier, M., Veit, S., Godt, A., Jeschke, G., and Spiess, H.W. (2000). Dead-time free measurement of dipole-dipole interactions between electron spins. J. Magn. Reson. *142*, 331–340.

Polyhach, Y., Bordignon, E., and Jeschke, G. (2011). Rotamer libraries of spin labelled cysteines for protein studies. Phys. Chem. Chem. Phys. *13*, 2356–2366.

Rodionov, D.A., Hebbeln, P., Eudes, A., ter Beek, J., Rodionova, I.A., Erkens, G.B., Slotboom, D.J., Gelfand, M.S., Osterman, A.L., Hanson, A.D., and Eitinger, T. (2009). A novel class of modular transporters for vitamins in prokaryotes. J. Bacteriol. *191*, 42–51.

Steinhoff, H.J., Radzwill, N., Thevis, W., Lenz, V., Brandenburg, D., Antson, A., Dodson, G., and Wollmer, A. (1997). Determination of interspin distances between spin labels attached to insulin: comparison of electron paramagnetic resonance data with the X-ray structure. Biophys. J. *73*, 3287–3298.

ter Beek, J., Duurkens, R.H., Erkens, G.B., and Slotboom, D.J. (2011). Quaternary structure and functional unit of energy coupling factor (ECF)-type transporters. J. Biol. Chem. *286*, 5471–5475.

Wang, J., Wolf, R.M., Caldwell, J.W., Kollman, P.A., and Case, D.A. (2004). Development and testing of a general amber force field. J. Comput. Chem. *25*, 1157–1174.

Zhang, P., Wang, J., and Shi, Y. (2010). Structure and mechanism of the S component of a bacterial ECF transporter. Nature *468*, 717–720.